Biomaterials Science

PAPER

View Article Online
View Journal | View Issue

Cite this: *Biomater. Sci.*, 2019, **7**, 2749

Folated pH-degradable nanogels for the simultaneous delivery of docetaxel and an IDO1-inhibitor in enhancing cancer chemo-immunotherapy†

Haishi Qiao,[a] Xingmei Chen,[a] Enping Chen,[a] Junmei Zhang,[a] Dechun Huang,*[a] Danqi Yang,[a] Youchao Ding,[b] Hongliang Qian,[a] Jan Feijen [c] and Wei Chen *[a]

Combining chemotherapy and immunotherapy has been considered as an attractive approach to improve cancer therapy. Here we prepared folated PVA-based nanogels for the simultaneous delivery of docetaxel (DTX) and the indoleamine 2,3-dioxygenase 1 (IDO1) inhibitor NLG919 (N9) for enhancing cancer chemo-immunotherapy. FDA-approved poly(vinyl alcohol) (PVA) with good biocompatibility was modified with vinyl ether acrylate (VEA) groups for UV-crosslinking and acidic degradation. Carboxyl groups were introduced *via* modification with succinic anhydride for improved drug loading and folic acid (FA) ligands were incorporated for tumor targeting. UV-crosslinked folated PVA nanogels were efficiently taken up by tumor cells followed by endo/lysosomal pH-triggered intracellular drug release, which induced significant cytotoxicity towards 4T1 breast cancer cells *in vitro*. DTX and N9 co-loaded PVA nanogels exhibited a much higher antitumor efficiency in 4T1 mouse breast cancer models *in vivo* as compared to the free drug controls. The drug-laden nanogels not only directly killed the tumor cells by DTX, but also induced immunogenic cell death (ICD) promoting intratumoral accumulation of cytotoxic T lymphocytes, and further combining with N9 elevated the intratumoral infiltration of CD8+ T cells and NK cells and inhibited the infiltration of MDSCs, downregulating IDO1-mediated immunosuppression.

Received 27th February 2019,
Accepted 4th April 2019

DOI: 10.1039/c9bm00324j

rsc.li/biomaterials-science

1. Introduction

Cancer chemotherapy, relying on cytostatic and/or cytotoxic effects, serves as a preferred clinical treatment for various types of cancers. Unfortunately, cancer treatment solely by chemotherapy is often insufficient to cure patients and always induces serious side effects due to nonspecific tumor targeting.[1] Tumor relapse commonly follows due to low drug penetration and undesirable tumor micro-metastases.[2,3] It is expected that a combination of cancer chemotherapy and immunotherapy would improve the patients' outcome, not only to deplete tumor cells, but also to prevent tumor relapse.[4]

It is evident that apoptosis and necrosis of tumor cells caused by chemotherapy are also able to stimulate the host immune system, in which immunogenic cell death (ICD) and neoantigen release from the cell debris contribute to the overall antitumor effects based on the characteristics of the specific anticancer immune responses.[5–7] The expression of calreticulin (CRT) on the surface of dead tumor cells introduced by ICD provides a "kill me" signal for antigen presenting cells (APC) and promotes the intratumoral infiltration of cytotoxic T lymphocytes (CTLs).[8] However, the activity of chemotherapy-induced immune responses is restricted by various negative feedback mechanisms such as immune checkpoints upregulated in the tumor immune environment.[9,10]

Interferon-γ (IFN-γ) secreted from CTLs up-regulates various immune checkpoints including indoleamine 2,3-dioxygenase 1 (IDO1) in tumors.[11] The overexpressed IDO1 within tumor cells and immune cells in the tumor environment is considered as an important negative feedback protein involved in facilitating tumor cell evasion from the immune system and promoting tumor growth and metastasis.[12,13] The depletion of tryptophan (Trp) catalyzed by IDO1 and accumulation of kynurenine (Kyn) impair the survival and activity of CD8+ T cells and suppress the antitumor immunity of CTLs.[14–19] The

[a]*Department of Pharmaceutical Engineering, School of Engineering, China Pharmaceutical University, Nanjing 210009, PR China. E-mail: cpuhdc@cpu.edu.cn, w.chen@cpu.edu.cn*
[b]*Industrial Products Inspection Center of Nanjing Customs, Nanjing 210019, P.R. China*
[c]*Department of Polymer Chemistry and Biomaterials, Faculty of Science and Technology, TECHMED Centre, University of Twente, P.O. Box 217, 7500 AE Enschede, The Netherlands*

†Electronic supplementary information (ESI) available. See DOI: 10.1039/c9bm00324j

IDO1-induced immunosuppressive microenvironment displays moderate tolerance to apoptotic cells as well as the activation of regulatory T cells (Tregs).[20–23] IDO1 inhibitors are used to pharmacologically inhibit the activation of IDO1 and improve the antitumor immunity as well as cancer chemotherapy.[12,13,24] For example, NLG919 (N9) as an important IDO1-selective inhibitor with a low half maximal effective concentration (EC50) value significantly reversed IDO1-mediated immune suppressive environments in preclinical models.[25] Therefore, strategies that are targeted to IDO1 inhibition combined with chemotherapy represent an attractive approach to enhance cancer chemo-immunotherapy by the combination of the ICD effect and antitumor immune response.

Nanomedicines as emerging platforms for cancer therapy are explored to improve pharmacological effects at the lesions by their distinct modalities and inherent physicochemical properties, while maximally reducing off-target side effects.[26] A promising approach is to design nanomedicines for the combination of chemotherapy and immune checkpoint inhibitors, such as IDO-1 inhibitors, for amplifying the cancer therapeutic benefits.[27–29] For example, Chen *et al.* developed a dual-functional immune-stimulatory micelle system based on a prodrug conjugate of PEG with N9 for the delivery of paclitaxel (PTX), by which the immuno-chemotherapy led to significant antitumor activity in both breast cancer and melanoma mouse models.[19] Feng *et al.* prepared pH and reduction dual-responsive binary cooperative prodrug nanoparticles (BCPNs) constructed from a self-assembled reducible N9 homodimer nanoparticle with a tumor acidity and reduction dual responsive oxaliplatin (OXA) prodrug as a coating for triggering ICD and eliciting antitumor immunity. Reduction-activated OXA promoted the intratumoral accumulation of CTLs by the ICD effect, and N9 downregulated IDO-1-mediated immunosuppression and suppressed Tregs.[25,30,31]

Nanogels constructed with a nano-sized three-dimensional (3D) network have been considered as promising candidates for controlled drug delivery, since they present several unique features such as a high water content, mechanical properties matched to the natural extracellular matrix (ECM), good biocompatibility, and excellent compatibility with different types of therapeutics including small molecule drugs and bio-macromolecules.[32] To improve the tumor targeting and controlled release profiles, bioresponsive nanogels decorated with targeting ligands could be rationally designed for enhanced cancer chemo-immunotherapy.[32–35] For example, Song *et al.* prepared a biomimetic nanogel based on hydroxypropyl-β-cyclodextrin/chitosan-based derivatives, shielded with an erythrocyte membrane for combinatorial chemotherapy and immunotherapy, in which the nanogel was able to deliver the immunotherapeutic agent interleukin-2 *via* the so-called 'nanosponge' properties, followed by precise pH-controlled intracellular release of PTX.[33] In this work, we designed folated pH-degradable PVA nanogels for the simultaneous delivery of docetaxel (DTX) and N9 to enhance cancer chemo-immunotherapy (Scheme 1). FDA-approved PVA with good biocompatibility and low toxicity

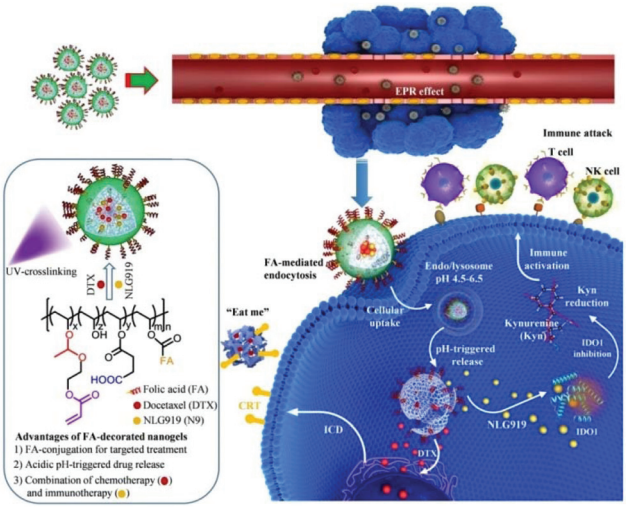

Scheme 1 Illustration of folated pH-degradable PVA nanogels (FA–NGs) for the simultaneous delivery of DTX and IDO1-inhibitor N9 in enhancing cancer chemo-immunotherapy.

was modified with vinyl ether acrylate (VEA) for UV-crosslinking, allowing acidic degradation, carboxyl groups *via* modification with succinic anhydride for improved drug loading, as well as folic acid (FA) ligand for tumor targeting. DTX and N9 were efficiently entrapped into the nanogels, and the folated nanogels significantly accumulated in tumor cells, strictly inhibiting premature drug release under physiological conditions. Dual drug loaded FA-NGs exhibited significant antitumor activity both *in vitro* and *in vivo* assisted by activating the innate and tumor-specific adaptive immune response through the promoted infiltration of CD8+ T cells and reduced distribution of immunosuppressive cells.

2. Experimental section

2.1. Materials

Ethylene glycol vinyl ether (98%), acryloyl chloride (98%), triethylamine (Et_3N, 99%), 2-hydroxy-4′-(2-hydroxyethoxy)-2-methylpropiophenone (I2959, 98%), succinic anhydride (99%), dicyclohexylcarbodiimide (DCC, 98%), 4-dimethylaminopyridine (DMAP, 97%), folic acid (FA, 97%), docetaxel (DTX, 99%), NLG919 (N9, 99.7%), and *p*-toluenesulfonic acid monohydrate (PTSA, 98%) were purchased from Energy Chemical Company and used as received. Polyvinyl alcohol (PVA, 87.0–89.0% hydrolyzed, M_n = 16 000, Acros). Vinyl ether acrylate (VEA) and VEA–functionalized PVA (PVA–VEA) were prepared according to the method given in our previous reports.[36] Carboxyl–functionalized PVA–VEA (PVA–VEA–COOH) was synthesized by adding PVA–VEA and succinic anhydride (molar of ratio of OH/succinic anhydride: 49/1) into DMSO and stirring at room temperature overnight using Et_3N as a catalyst. FA–decorated PVA–VEA–COOH (FA–PVA–VEA–COOH) was prepared by adding PVA–VEA–COOH and FA (molar ratio of OH/FA: 16/1) into DMSO and stirring at room temperature

overnight. The functionality degree of VEA, COOH and FA groups on PVA was determined as 2.7, 2.1 and 1.6% by ^{1}H NMR analysis, respectively, which was performed on a Bruker ACF-300Q spectrometer (USA). For cell culture experiments, HeLa and 4T1-Luc cells were cultured in Dulbecco's modified Eagle's medium (DMEM) with high glucose, supplemented with 10% heat inactivated fetal bovine serum, 2 mM L-glutamine, nonessential amino acids, and sodium pyruvate (the medium and supplements are from Life Technologies). Cells were cultured at 37 °C in a humidified atmosphere with 5% CO_2.

2.2. Characterization

The size of the nanogels was determined by dynamic light scattering (DLS) at 25 °C using an Anton Paar Litesizer 500 equipped with a 658 nm laser. Transmission electron microscopy (TEM) was performed using a FEI Philips Tecnai 20 under an acceleration voltage of 80 kV. The TEM samples were prepared by dropping 10 μL of nanogel (1.0 mg mL^{-1}) on a copper grid followed by lyophilization.

2.3. Nanogel preparation and drug encapsulation

PVA–VEA–COOH or FA–PVA–VEA–COOH was dissolved in water at a concentration of 1.0 mg mL^{-1} with I2959 as a photoinitiator (5 wt% of polymer) at room temperature, and polymer nano-precursors formed by adjusting the solution pH to 6.5 were exposed to UV (20 mW cm^{-2}) for 10 min under continuous stirring to form nanogels. To prepare N9 and DTX loaded nanogels, an aqueous polymer solution (1.0 mg mL^{-1}) was combined with N9 and DTX (50 mg mL^{-1} separately in ethanol) as well as I2959 (5 wt% of polymer), followed by UV-exposure for nanogel crosslinking. The drug feeding ratio was set at 10 wt% of the polymer, and the free drug was removed by centrifugation with a molecular weight cut off (MWCO) of 10 000.

2.4. pH-Induced degradation of nanogels and *in vitro* release of N9

PVA nanogels (1.0 mg mL^{-1}) were separately suspended in phosphate buffer (PB, pH 7.4) and acetate buffer (pH 5.0), and the size change of the nanogels under slow shaking at 37 °C was monitored over time by DLS to determine the nanogel degradation. The *in vitro* release of N9 from nanogels was studied using either PB (pH 7.4) or acetate buffer (pH 5.0) at 37 °C. Two aliquots of N9-loaded nanogels (1.0 mg mL^{-1}) were transferred to a dialysis tube with a MWCO of 12 000–14 000, and placed into 20 mL of appropriate buffers. At the desired time intervals, 5.0 mL of release medium was taken out from each group and replenished with an equal volume of corresponding fresh medium. The release medium was freeze-dried and the amount of N9 was determined by HPLC according to a standard curve (Ultramate 3000, Thermo Fisher, USA) with UV detection at 262 nm using 0.1% H_3PO_4 in 100% acetonitrile. Release experiments were conducted in triplicate, and the results are presented as the average ± standard deviation.

2.5. Intracellular uptake of nanogels

FITC was introduced to nanogels *via* an ester condensation reaction between the isothiocyanate groups of FITC and the hydroxyl groups of F-NGs in DMSO. Free FITC was removed by centrifugation with a MWCO of 10 000. HeLa cells were seeded on microscope slides in a 24-well plate (1.0×10^4 cells per well) using DMEM containing 10% FBS. After 12 h incubation, 50 μL of FITC-labeled nanogel samples (1.0 mg mL^{-1}) were added into the culture medium. After 4 h incubation, the culture medium was removed and the cells were washed twice with phosphate buffered saline (PBS). The cells were then fixed with 4% paraformaldehyde for 20 min, incubated with DAPI (Beyotime Biotechnology, China) to stain the cell nucleus at room temperature for 10 min. Fluorescence images of cells were obtained with a fluorescence microscope (IX73, Olympus, Japan) and analyzed by ImageJ software. Flow cytometry analysis was performed to quantify the cellular uptake of nanogels. HeLa cells were cultured in a 24-well plate (1.0×10^5 cells per well) for 12 h followed by the treatment as mentioned above. After 4 h incubation, the culture medium was removed, and the cells were rinsed thrice with PBS and treated with trypsin. The cell suspensions were washed twice with PBS and re-suspended in PBS. The quantification of fluorescence was performed by using a FACSCalibur (BD Accuri C6).

2.6. Western blot analysis

Cells were lysed in a buffer containing 50 mM Tris-HCl (pH 7.4), 150 mM NaCl, 1 mM sodium vanadate, 1% Nonidet P-40, and protease inhibitors (Selleck, Shanghai, China). The cell lysates were centrifuged at 10 000*g*, and the supernatants were added to the loading buffer and separated by SDS-PAGE. After being transferred to a polyvinylidene difluoride membrane (Roche, USA), 1 : 1000 of IDO1 antibody (Cell Signaling Technology) was used to detect the proteins followed by HRP-conjugated secondary antibody and the ECL reagent kit treatment (Tanon, China). The images were collected using an Alpha Innotech Fluor Chem FC2 imaging system (Gel Doc™ EE imager, CA, USA).

2.7. *In vitro* IDO1 assay

The inhibitory activity of FA–NGs–N9 on IDO1 was evaluated by an *in vitro* IDO1 assay.[13] Briefly, HeLa cells were cultured in a 24-well plate at a cell density of 5×10^5 cells per well for 12 h. After that, recombinant human IFN-γ (Sino biological, Beijing, China) was added into the culture medium with a final concentration of 50 ng mL^{-1} followed by the addition of various concentrations of free N9, NGs–N9, and FA–NGs–N9. After 72 h incubation, two aliquots of 200 μL of the supernatants from each well were transferred to an 1.5 mL EP tube, followed by the addition of 100 μL of 30% trichloro-acetic acid and incubation for 30 min at 50 °C to hydrolyze *N*-formylkynurenine to kynurenine. The supernatants after centrifugation with 10 000*g* were measured by colorimetric assay and HPLC. For the colorimetric assay, samples were transferred to a 96-well plate, mixed with Ehrlich reagent (2% *p*-dimethylamino-benz-

aldehyde in glacial acetic acid, w/v), and incubated for 10 min at room temperature. The results were measured at 490 nm using a plate reader and calculated according to a standard calibration curve. For the HPLC assay, the hydrolysis product of kynurenine was directly analyzed at a wavelength of 355 nm.

2.8. T-cell proliferation evaluation

Splenocyte suspensions were collected from BALB/c mice by using the lymphocyte separation liquid (TBD science, China), and the cells were vigorously suspended in erythrocyte lysis buffer (Beyotime Biotechnology, Nantong, China), and then incubated for 3 min at room temperature. The cell suspensions were filtered through a fresh cell strainer and then passed through a nylon wool column and washed with RPMI1640 media. The T cells were collected by centrifugation and re-suspended in RPMI1640 media for the following co-culture experiment. The co-culture of HeLa or 4T1-Luc with T cells was performed to determine IDO1-mediated T cell proliferation inhibition which can be reversed by IDO1 blockade. HeLa and 4T1-Luc cells were separately cultured in 24 well plates for 12 h, and then co-incubated with T cells pre-stained with 5-(and 6)-carboxyfluorescein diacetate (CFSE, LOT.4341058, eBioscience, USA). The medium was supplied with 50 ng mL^{-1} of IFN-γ, 100 ng mL^{-1} of anti-CD3 (LOT.4335068, eBioscience, USA) and 10 ng mL^{-1} of mouse recombinant IL-2 (LOT.0717108, Pepro Tech, China), followed by the addition of various concentrations of free N9, NGs–N9 or FA–NGs–N9. T-cell proliferation was measured by using a FACSCalibur after co-culture for 3 days.

2.9. Cell viability test

Cell viability and half maximal inhibitory concentration (IC50) values mediated by the drug-loaded nanogels were measured by the MTT assay. 4T1-Luc cells were seeded on a 96-well plate at a density of 5×10^3 cells per well and incubated with 5% CO_2 at 37 °C. After 12 h, the cells were treated with different concentrations of free N9, free DTX, NGs–D–N9, or FA–NGs–D–N9 and incubated for 24 h. After that, 10 μL of MTT (5.0 mg mL^{-1}, Sigma Aldrich, St Louis, USA) was added to each well and the cells were incubated for another 4 h. The medium was replaced by 100 μL of DMSO to dissolve the resulting purple crystals. The absorbance was measured at 570 nm in a microplate reader (Molecular Devices, silicon vallery, CA, USA) and the data were used to extrapolate IC50 values. To further investigate the effect of FA-decoration on the cytotoxicity of the drug loaded nanogels, the cells were pre-treated with 10 μL of free folic acid (10 mg mL^{-1}) for 4 h, and then the medium was replaced by fresh medium containing free DTX, NGs–D–N9, or FA-NGs–D–N9 and incubated for 24 h. After that, the cell treatment procedure was carried out as mentioned above to test the cytotoxicity. The experiments were conducted in triplicate, and the results are presented as the average ± standard deviation.

2.10. *In vivo* imaging of FA–NGs

In vivo bio-distribution of FA–NGs is demonstrated using 4T1-Luc cells bearing BALB/c mice obtained from the Model Animal Research Centre of Nanjing University (Nanjing, China). All animal experiments were carried out in compliance with the Animal Management Rules (Ministry of Health, People's Republic of China) and the guidance for Care and Use of Laboratory Animals (China Pharmaceutical University). In order to monitor the *in vivo* fluorescence imaging of nanogel samples, DiR was loaded into NGs or FA–NGs with a final DiR concentration of 20 μg mL^{-1}. The 4T1-Luc murine breast cancer xenograft model was established by subcutaneous inoculation of 4T1-Luc tumor cells (2×10^5 cells per mouse) into female BALB/c mice. After 15 d, the tumor size approximately reached 150–200 mm^3, and the tumor-bearing mice were randomly grouped and injected with 200 μL of DiR-loaded NGs or FA–NGs *via* the tail vein. At predetermined time points (2, 4, 8, and 24 h) post i.v. injection, the mice were anesthetized with isoflurane and then the fluorescence images were acquired. The main organs were also dissociated after euthanasia for *ex vivo* fluorescence imaging. The fluorescence images were scanned using a near-infrared fluorescence imaging system (IVIS® Lumina™, USA) at an excitation of 747 nm and emission of 774 nm, and the images were acquired and analyzed using Lumia II software.

2.11. *In vivo* antitumor efficacy of FA–NGs–D–N9

The *in vivo* antitumor activity of drug-loaded nanogels was examined using a 4T1-Luc murine breast cancer xenograft mouse model. Treatment started after 1 week when tumors reached a size of 30–50 mm^3, and this day was designated as day 0. The mice were weighed and randomly divided into six groups ($n = 6$): PBS, FA–NGs, free DTX, free N9, combination of DTX and N9, and FA–NGs–D–N9. The formulations at a dosage of 10 mg of DTX and 21 mg of N9 equiv. kg^{-1} were i.v. injected *via* the tail vein. The tumor size was measured using a Vernier caliper every 3 d and the tumor volume was calculated according to the formula $V = 0.5 \times L \times W^2$, wherein L and W were the tumor dimensions at the longest and widest, respectively. The relative tumor volume was calculated as V/V_0 (V_0 is the tumor volume at day 0). The relative body weight of the mice was normalized to their initial weight (w/w_0, w_0 is the body weight at day 0). At the end of the experiments, the bioluminescence intensity of the tumor-bearing mice was imaged by using an IVIS device after the injection of D-luciferin potassium salt. Subsequently, all the mice were euthanatized, and the tumor tissues were imaged by photography, analyzed by flow cytometry, hematoxylin–eosin (HE) staining and immunohistochemistry (IHC). The normal tissues of excised heart, liver, spleen, lung and kidney were fixed with 4% paraformaldehyde solution and embedded in paraffin. The sliced organ tissues (thickness: 4 mm) on the glass slides were stained by HE and observed with a digital microscope (ECLIPSE Ci-L, Nikon, JAPAN).

2.12. Quantification of tumor-infiltrating lymphocytes

At the end of different treatments of the 4T1-Luc tumor-bearing BALB/c mice, the eviscerated tumor tissues were cut into smaller pieces and digested in 1640 medium with 0.5 mg

mL^{-1} collagenase type IV for 1 h at 37 °C. The digested tissues were gently meshed through a 70 μm cell strainer and collected by using the lymphocyte separation liquid. The cell suspensions were stained with various combinations of fluorophore-conjugated antibodies for 30 min at 4 °C. The immune cells were stained with anti-CD45–Cy5.5 (BioLegend, LOT: 103132, clone: 30-F11), anti-CD8a-PE (eBioscience, LOT: 4335056, clone: 53–6.7), anti-CD49b–PE (Invitrogen, LOT: 1930449, clone: DX5), CD11b–FITC (eBioscience, LOT: 4306305, clone: M1/70) and Ly6G–PE (BD Pharmingen, LOT: 561084, clone: RB6-8C5) antibodies according to the manufacture's protocols. After washing, the cells were used for flow cytometry analysis (Beckman, Cytoflex FCM, USA). The data were processed by FlowJo software.

3. Results and discussion

3.1. Preparation of folated pH-degradable PVA nanogels (FA–NGs)

VEA-functionalized PVA was prepared *via* acetalization in anhydrous DMSO using a catalytic amount of PTSA according to our previous report,[36] followed by the reaction with succinic anhydride to introduce carboxyl groups for improved drug loading, and conjugation with the FA ligand for tumor targeting (Fig. S1†). The aqueous FA–PVA–VEA–COOH solution was firstly adjusted to a pH of 6.5 to form nanoaggregates, followed by UV-exposure to crosslink VEA units *via* the double bonds for nanogel preparation. The acetal linker was used for realizing acidic pH-induced nanogel dissociation and drug release. The average size of FA-decorated PVA nanogels (FA–NGs) was 84 nm with a narrow PDI of 0.05 determined by DLS, which was in line with the TEM observation (Fig. 1A). The crosslinked nanogels were characterized by FT-IR, where the peak at 1645 cm^{-1} attributed to the double bond of VEA units disappeared after UV irradiation, demonstrating the successful UV-crosslinking (Fig. S2A†). Because of the crosslinked structure, the nanogels displayed swelling behaviour in DMSO instead of dissolution into a unimolecular structure (Fig. S2B†). PVA nanogels without FA decoration (NGs) prepared *via* the same method were used as a control and the size was about 132 nm (Fig. S3†). The IDO1 inhibitor N9 and the anticancer drug DTX could be conveniently loaded into FA–NGs during their formation. The size of the drug loaded FA–NGs was also measured by DLS. N9-loaded FA–NGs (FA–NGs–N9) had a size around 83 nm and DTX–loaded FA–NGs (FA–NGs–D) exhibited a size of 71 nm (Fig. 1B). N9 and DTX co-loaded FA–NGs had a smaller size of about 65 nm which was most probably due to the strong hydrophobic interactions between drugs and nanogels. The loading efficiency (LE) of N9 and DTX into FA–NGs could reach up to 83% and 60%, respectively, at a theoretical LC of 10 wt%. The LE was still good when these two drugs were co-loaded into nanogels (denoted as FA–NGs–D–N9). It is interesting that FA–NGs showed a higher loading capacity for both N9 and DTX compared with NGs (Table S1†).

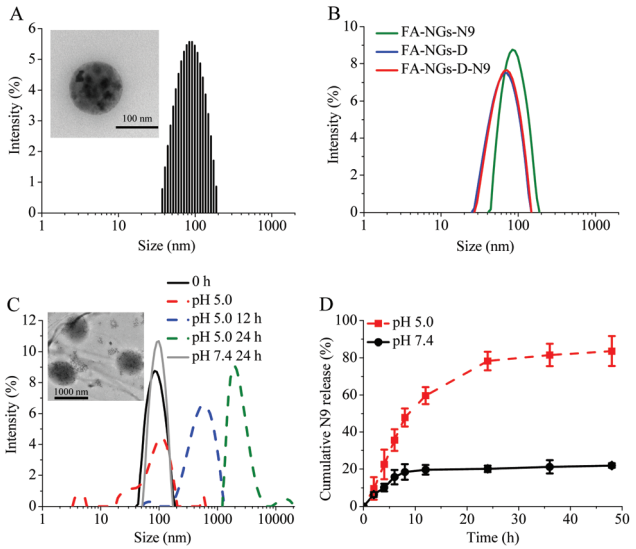

Fig. 1 Characterization of folated pH-degradable PVA nanogels. (A) Size distribution of FA-NGs determined by DLS (insert: TEM image of FA–NGs stained with phosphotungstic acid) and (B) size distribution of N9 and DTX loaded FA–NGs, respectively; (C) pH-induced size change of FA–NGs over time monitored by DLS (insert: TEM image of FA–NGs after 24 h degradation in pH 5.0) and (D) pH-triggered cumulative N9 release from FA–NGs at 37 °C.

To demonstrate the pH-sensitivity of nanogels, FA–NGs were subjected to different pH conditions and the size was monitored by DLS over time. FA–NGs at pH 5.0 showed rapid and dramatic swelling, in which the size increased from 84 nm to about 586 nm in 3 h, reaching over 1000 nm after 6 h (Fig. 1C). There were still big nanoparticles after 24 h degradation in pH 5.0, which is mostly attributed to the incomplete acetal hydrolysis, as well as the strong hydrogen bonding from the OH groups of PVA, resulting in the large swelling of the nanogels. It is interesting to note that the size of FA-NGs remained unchanged after 24 h incubation at pH 7.4. Because of the fast swelling and dissociation of nanogels due to the acetal hydrolysis at acidic pH, the *in vitro* release of N9 from FA-NGs was also accelerated in acidic pH. As displayed in Fig. 1D, a minimal amount of N9 (12.6%) was released from FA–NGs at physiological pH for 12 h, and less than 20% was detected after 48 h. However, more than 40% of N9 was released in 12 h at pH 5.0, and the released amount reached up to 65% in 24 h. Previously, a similar pH-controlled release behavior of PTX from PVA–VEA nanogels has been measured.[33]

3.2. Cellular uptake of FA–NGs

To demonstrate that FA–NGs could be more efficiently internalized by cells *via* FA receptor mediated endocytosis than non-modified nanogels, the cellular uptake behavior of FITC-labeled nanogels was investigated by fluorescence microscopy. FITC–labeled FA–NGs were well distributed in HeLa cells after only 4 h incubation, while non-modified NGs displayed a significantly weaker FITC intensity in the cells than FA–NGs (Fig. 2A). The cellular uptake of FITC-modified nanogels was

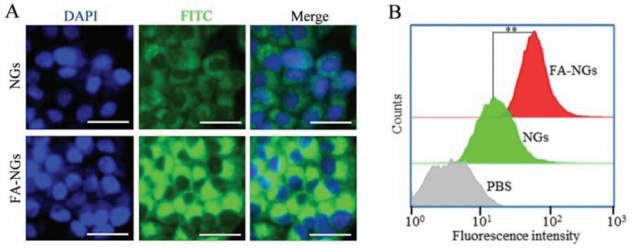

Fig. 2 Intracellular uptake of FITC-labeled PVA nanogels in HeLa cells. (A) Fluorescence images of HeLa cells after 4 h incubation with NGs and FA–NGs (0.5 mg mL^{-1}). The images show for each panel from left to right cell nuclei stained by DAPI (blue), FITC-labeled nanogels (green) in cells, and overlays of two images (scale bar: 50 μm); (B) flow cytometry profiles of HeLa cells after 4 h incubation with FITC-labeled NGs and FA–NGs (the cells treated with PBS were used as a blank control, $^{**}p < 0.01$).

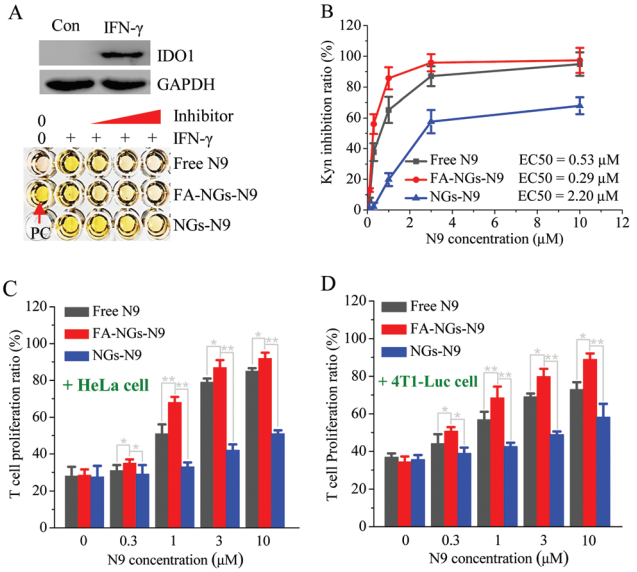

Fig. 3 (A) Western blot analysis of IDO1 expression in HeLa cells pre-incubated with IFN-γ for 24 h (upper panel), and the colorimetric assay of Kyn inhibition after the addition of free N9, FA–NGs–N9 and NGs–N9 (lower panel, free Kyn was used as a positive control (PC)); (B) Kyn inhibition ratio and EC50 values calculated according to the colorimetric assay (HeLa cells pre-incubated with IFN-γ used as a positive control). (C and D) T cell proliferation by incubation with HeLa (C) and 4T1-Luc (D) cells determined by FACS analysis. HeLa cells and 4T1-Luc cells were separately co-cultured with splenocytes, and then treated with IL-2, anti-CD3 antibody, anti-CD28 antibody and IFN-γ, followed by the addition of free N9, FA–NGs–N9 or NGs–N9, and incubation for another 3 days. The T cells were stained with CFSE (carboxyfluorescein succinimidyl ester). All results are based on three independent experiments. The data are presented as the average ± standard deviation (n = 3, $^{*}p < 0.05$, $^{**}p < 0.01$).

further quantified by flow cytometry analysis. As expected, the flow cytometry results showed that HeLa cells following 4 h treatment with FA–NGs displayed a 3.7-fold higher fluorescence intensity than cells incubated with NGs (Fig. 2B), indicating an enhanced cellular uptake of the FA ligand modified NGs.

3.3. *In vitro* IDO1 inhibition by N9–loaded FA–NGs

Inhibition of IDO1 was selected as a means to stimulate the immune system to recognize and attack tumor cells, because the degradation of Trp into Kyn catalyzed by IDO1 impairs the survival and the activity of immune cells.[37] It has been reported that N9 has super targetability towards IDO1 and significantly inhibits the oxidation of the essential amino acid Trp.[38,39] The inhibition activity of N9-loaded nanogels in HeLa cells was determined by the amount of Kyn converted from Trp. HeLa cells were treated with IFN-γ to induce IDO1 expression (Fig. 3A, upper panel), followed by the treatment with different N9 formulations, and the amounts of Kyn in culture medium were determined by HPLC (Fig. S4A†) and colorimetric assay (Fig. 3A, lower panel). As shown in Fig. 3B, the level of Kyn induced by IDO1 decreased in a concentration-dependent manner to N9 treatment. Due to the FA-mediated endocytosis, FA–NGs–N9 exhibited the most efficient inhibition of IDO1 activity with an EC50 of 0.29 μM, while the EC50 of NGs–N9 and free N9 was 2.2 μM and 0.53 μM, respectively. NLG919 is a highly IDO1-selective inhibitor and the EC50 is determined as 75 nM by the standard enzymatic assay. However, the efficiency of IDO1 inhibition by NLG919 under the intracellular conditions is much different from that by the standard enzymatic assay, in which the inhibitor could possibly react with many other target proteins, significantly increasing the EC50 value.[40] The resulting Kyn production was also quantified by HPLC, which was in line with the colorimetric assay (Fig. S4B†).

T cell proliferation could be inhibited by co-culture with IDO1-overexpressed tumor cells. Once the IDO1 activity is blocked in tumor cells, it would be possible to reverse the inhibition of T cells. As shown in Fig. 3C, T cells isolated from splenocytes in BALB/c mice were co-cultured with IDO1 overexpressing HeLa cells, which were obtained by stimulation with IFN-γ, and the proliferation of the T-cells was strongly inhibited. This inhibition was significantly attenuated when the co-culture system was treated with free N9 or N9-loaded nanogels, in which the inhibition efficiency was also dependent on the N9 concentration (Fig. 3C). It was found that FA–NGs–N9 displayed dramatically higher activity to reverse the inhibitory effect compared with other groups. We further co-cultured T cells with mouse breast cancer cell line 4T1-Luc cells, in which murine IFN-γ was used to induce the overexpression of IDO1 in 4T1-Luc cells. The result showed that FA–NGs–N9 also mediated strong IDO1 inhibition, and significantly activated T cell proliferation, which was consistent with previous results (Fig. 3D).

3.4. *In vitro* cytotoxicity of FA–NGs–D–N9

Since IDO1 pathway inhibition exhibits a promising prospect on immune checkpoint blockade, chemotherapy combined with immunotherapy represents an attractive approach for synergetic cancer therapy. First, the cytotoxicity of blank FA–

NGs and NGs was evaluated by MTT assay using 4T1-Luc cells. We demonstrated that both nanogels were practically nontoxic (cell viabilities ≥90%) up to a concentration of 1.0 mg mL^{-1} (Fig. S5A†), and N9–loaded FA–NGs and NGs also showed no toxicity towards 4T1-Luc cells up to a N9 concentration of 160 ng mL^{-1} (Fig. S5B†). However, the cell viability of 4T1-Luc cells treated with nanogels at different concentrations of DTX significantly decreased, in which FA–NGs–D–N9 exhibited efficient cell inhibition with an IC50 value of 45.6 ng mL^{-1}, that was much lower than that of free DTX or NGs–D–N9 (Fig. 4A). To confirm that the enhanced inhibition effect towards tumor cells was mediated by the FA targeting ligand, 4T1-Luc cells were pretreated with free FA to block the FA receptor. As shown in Fig. 4B, the antitumor activity of FA–NGs–D–N9 obviously decreased by free FA treatment, while no influence was observed when using NGs–D–N9 or free DTX. It should be noted that the cytotoxicity of DTX was not enhanced by the co-delivery of N9 and DTX through FA–NGs as compared to only DTX–loaded FA–NGs, which implies that possible antitumor effects induced by IDO1 inhibition can be attributed to an improved immune response *in vivo*.

3.5. *In vivo* antitumor activity of DTX and NLG919 loaded NGs

In vivo tumor-targetability was investigated using 4T1-Luc breast tumor-bearing BALB/c mice, which were i.v. injected with 1,1′-dioctadecyltetramethyl indotricarbocyanine iodide (DiR)-loaded nanogels and monitored by using a near-infrared fluorescence imaging system over time. As shown in Fig. S6,† DiR–loaded FA–NGs exhibited obvious higher fluorescence in the tumor tissues than NGs in both *in vivo* and *ex vivo* organs. The therapeutic performance of DTX and N9 co-loaded FA–NGs was evaluated using the 4T1-Luc mouse breast cancer model. The mice were treated with free DTX, free N9, free DTX and N9, and DTX and N9 loaded FA–NGs by i.v. injection when palpable tumor masses reached a size of 30–50 mm^3. Tumor growth and mouse weight were monitored every three days for different treatments (Fig. 5A). The results showed that

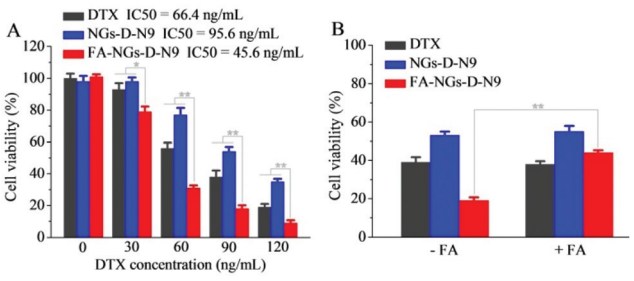

Fig. 4 Cytotoxicity of DTX-loaded nanogels using 4T1-Luc cells determined by MTT assay. (A) Cell viability of 4T1-Luc cells incubated with nanogel samples at different concentrations of DTX for 24 h; (B) cell viability of 4T1-Luc cells pretreated with free FA (1.0 mg mL^{-1}) for 4 h, followed by 24 h incubation with fresh culture medium containing nanogel samples at a DTX concentration of 90 ng mL^{-1}. All results are based on three independent experiments. The data are presented as the average ± standard deviation (n = 3, *p < 0.05, **p < 0.01).

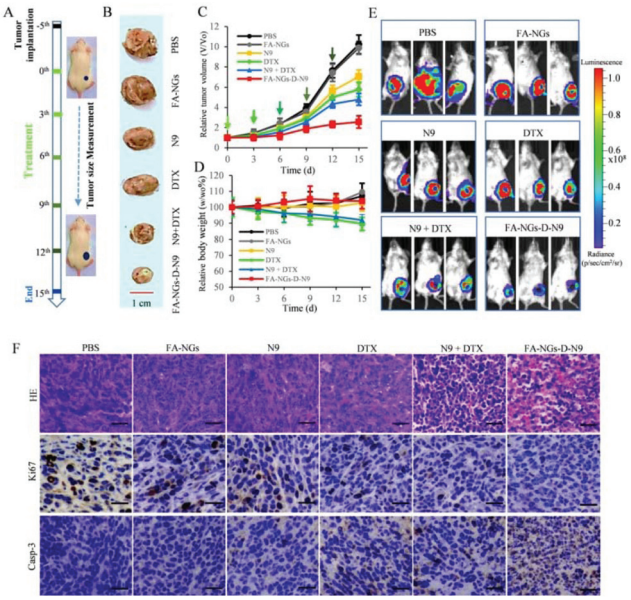

Fig. 5 *In vivo* antitumor performance in 4T1-Luc tumor-bearing BaLB/c mice (n = 6) by i.v. injection with different samples. (A) Administration schedule for *in vivo* therapy on 4T1-Luc tumor-bearing BaLB/c mice by i.v. injection with PBS, blank FA-NGs, free DTX, free N9, free DTX & free N9, and DTX/N9-loaded FA-NGs (DTX: 10 mg kg^{-1}; N9: 21 mg kg^{-1}). The injections were performed on day 0, 3, 6, 9, and 12. (B) Representative tumor images from each group after euthanizing the animal on day 15. (C) Tumor volume changes of mice with different treatments. (D) Body weight changes of mice in different treatment groups within 15 days. (E) *In vivo* imaging was performed on day 15 to monitor tumor growth. (F) Histological examination including H&E staining images and IHC staining images of Ki-67 and cleaved caspase-3 of 4T1-Luc tumors from tumor-bearing BaLB/c mice after 15 days with different treatments. The data are presented as the average ± standard deviation (n = 6).

free DTX, free N9 and a combination of DTX and N9 could significantly inhibit the tumor growth but FA–NGs–D–N9 revealed the most therapeutic efficacy by the comparison of continuous tumor growth in the treatment groups. The relative tumor volumes at 15 d were 10.0, 9.9, 7.1, 5.8, 4.8, and 2.6 for mice treated with PBS, blank FA–NGs, N9, DTX, combination of N9 and DTX, and FA–NGs–D–N9, respectively (Fig. 5B and C). Mice treated with free DTX or free DTX+ N9 showed obvious weight loss during the treatment time while FA–NGs loaded with DTX and N9 caused little change of body weight indicating that DTX carried by FA–NG carriers had little systemic toxicity (Fig. 5D).

Living imaging was performed to detect the luminescence intensity representing the tumor growth of mice bearing 4T1-Luc cells at day 15. Treatment with FA–NGs–D–N9 resulted in significant tumor shrinkage with much weaker luminescence intensity compared to other groups (Fig. 5E). At the end of the experiment, all the mice were euthanized to analyze the tumor with HE staining or immunohistochemistry (IHC), which revealed that FA–NGs–D–N9 caused more inhibition of tumor cell proliferation indicated by Ki67 reduction and increased tumor cell apoptosis as indicated by the cleaved caspase-3 protein elevation compared to other treatments (Fig. 5F). The

H&E staining also revealed that FA–NGs–D–N9 caused more necrosis in the tumor tissue but less damage to heart and lung tissues without inflammatory changes, cell degeneration or cell death, demonstrating that drug laden FA–NGs were able to reduce adverse drug effects (Fig. 5F and S7†).

3.6. *In vivo* immune performance

It is reported that chemotherapeutic agents such as DOX, OXA and PTX not only can directly kill tumor cells through inducing cell apoptosis but also may elicit antitumor immunity by inducing ICD, characterized by the secretion of damage-associated molecular patterns, which promotes the intratumoral infiltration of CTLs.[41,42] Preclinical and clinical studies demonstrated that DTX treatment or a combination with antitumor vaccine exhibited a potential benefit in cancer immunotherapy, since DTX induced CRT exposure on the cell surface and initiated the ICD cascade of the tumor cells, resulting in increased immunogenicity.[43–47] Additionally, developing advanced nanocarriers that deliver taxane agents is also able to initiate ICD responses for cancer immunotherapy.[48] We performed IHC to detect whether DTX treatment could increase the expression of CRT on the apoptotic cell surface functioning as "danger signals" for the immune system for recognition and processing by antigen-presenting cells. As shown in Fig. 6A, DTX treatment can significantly induce the expression of CRT and IFN-γ in tumor tissues which can be enhanced by IDO1 inhibition. FA–NG-mediated delivery of DTX and N9 showed the strongest expression of CRT and IFN-γ. Immunohistochemistry images showed that IDO1 blockage significantly increased the expression of HMGB-1 caused by DTX in tumor tissues, which paralleled with the increase in CRT. The mechanism of the enhanced effect for ICD is highly complicated, and here it might be because that IDO1 inhibition would reprogram the tumor immune microenvironment and strengthen the immune response to the immunogenicity of tumor cell death induced by antineoplastics.[25,30] The HMGB-1 levels did not become elevated after treatment with single N9, PBS or blank FA–NG controls. It should be noted that FA–NGs–D–N9 treatment induced more abundant expression of HMGB-1 as compared to the other groups.

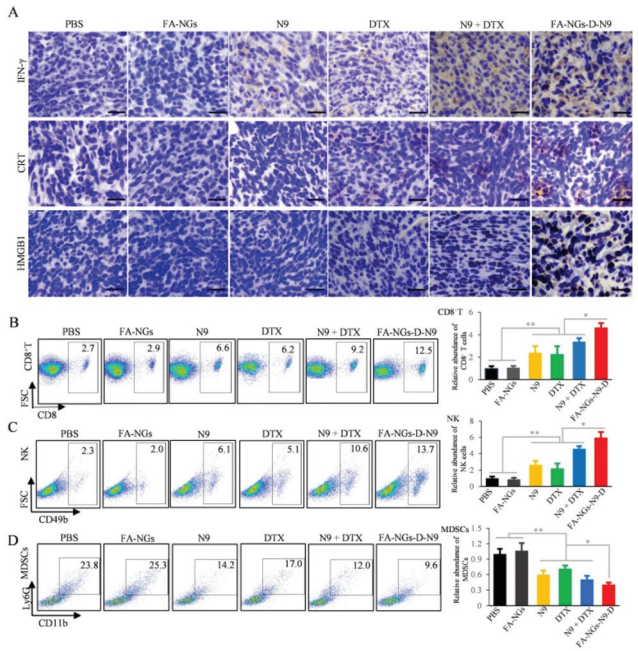

Fig. 6 Immunohistochemistry analysis and flow cytometry of immune cell subsets from the tumor tissues after different treatments for 15 days. (A) Immunohistochemistry images of the expression of IFN-γ, CRT and HMGB-1. Flow cytometry analysis of CD45+ cells stained with CD8 antibody (B), CD49b antibody (C) and CD11b and Ly6G antibody (D). CD45+ cells were lymphocytes isolated from tumor tissues using the lymphocyte separation liquid and stained with CD45 antibody. The data are presented as the average ± standard deviation (n = 3, *p < 0.05, **p < 0.01).

To further confirm chemo-immunotherapy mediated by a combination of DTX and N9 assisted by FA–NGs, the immune cell population in the tumor tissues was analyzed by flow cytometry to assess the immune response mediated by different treatment groups for five times. The infiltration of CD8+ T cells in the tumors was significantly increased in all of the treatment groups compared with blank nanogels or PBS groups (Fig. 6B). However, there were significantly more CD8+ T cells in the tumors treated with FA–NGs–D–N9 compared with a combination of N9 and DTX without nanogels. It is reported that the depletion of Trp mediated by IDO1 not only could impair the survival and activity of CD8+ T cells but also impair NKp46/NKG2D-specific lysis of NK cells *via* the formation of Kyn.[49,50] IDO1 inhibition would also reduce the number of myeloid-derived suppressor cells (MDSCs) in the tumors.[46,51] Based on this, the population of NK cells in the tumor tissue was also quantified by FACS. As shown in Fig. 6C, FA–NGs–D–N9 exhibited the strongest inhibition of IDO1 and resulted in the elevation of NK cells to infiltrate the tumor tissue, as compared to other treatment groups. Meanwhile, FA–NGs–D–N9 treatment also exhibited the strongest inhibition of MDSCs in the tumor tissues (Fig. 6D), which indicated that the IDO1 inhibitor N9 delivered by FA–NGs significantly inhibited the immunosuppression in the tumor microenvironment.

4. Conclusions

We have demonstrated folated pH-degradable PVA nanogels for the simultaneous intracellular delivery of DTX and the IDO1-inhibitor N9, mediating enhanced cancer chemo-immunotherapy on 4T1 breast cancer by activating the ICD mechanism and reversal of IDO1-related immune-suppressive effects. These nanogels with a well-defined crosslinked structure showed excellent colloidal stability for both DTX and N9 loading but rapid degradation and a pH-triggered release under intracellular acidic conditions. The FA ligand promoted the cellular uptake of the nanogels and an enhanced tumor immunogenicity was introduced by the ICD cascade of the tumor cells caused by DTX. Meanwhile, the IDO1 inhibitor N9

elevated the intratumoral infiltration of CD8+ T cells and NK cells, and also hampered the infiltration of MDSCs, reversing the IDO1-mediated immunosuppressive tumor microenvironment. We are convinced that our PVA-based degradable nanogel system provides a promising template with a high potential for the treatment of different malignant tumors by combinatorial chemo-immunotherapy.

Conflicts of interest

There are no conflicts to declare.

Acknowledgements

This work was supported by the National Key Research and Development Program of China (No. 2017YFD0401301), the National Natural Science Foundation of China (NSFC 51703244, 81600178, 21878337, 21676291), the Natural Science Foundation of Jiangsu Province (BK20170730), Jiangsu Agriculture Science and Technology Innovation Fund (JASTIF CX(18)3039), Leading Talents in Schoow Technological Innovation and Entrepreneurship (WC201816) and the Jiangsu Specially-Appointed Professor Program to W. C.

Notes and references

1 L. Bracci, G. Schiavoni, A. Sistigu and F. Belardelli, *Cell Death Differ.*, 2014, **21**, 15–25.
2 S. Torok, M. Rezeli, O. Kelemen, A. Vegvari, K. Watanabe, Y. Sugihara, A. Tisza, T. Marton, I. Kovacs, J. Tovari, V. Laszlo, T. H. Helbich, B. Hegedus, T. Klikovits, M. A. Hoda, W. Klepetko, S. Paku, G. Marko-Varga and B. Dome, *Theranostics*, 2017, **7**, 400–412.
3 M. de Boer, C. H. van Deurzen, J. A. van Dijck, G. F. Borm, P. J. van Diest, E. M. Adang, J. W. Nortier, E. J. Rutgers, C. Seynaeve, M. B. Menke-Pluymers, P. Bult and V. C. Tjan-Heijnen, *N. Engl. J. Med.*, 2009, **361**, 653–663.
4 C. Wang, W. Sun, G. Wright, A. Z. Wang and Z. Gu, *Adv. Mater.*, 2016, **28**, 8912–8920.
5 L. Zitvogel, L. Apetoh, F. Ghiringhelli, F. Andre, A. Tesniere and G. Kroemer, *J. Clin. Invest.*, 2008, **118**, 1991–2001.
6 L. Bezu, A. Sauvat, J. Humeau, L. C. Gomes-da-Silva, K. Iribarren, S. Forveille, P. Garcia, L. Zhao, P. Liu, L. Zitvogel, L. Senovilla, O. Kepp and G. Kroemer, *Cell Death Differ.*, 2018, **25**, 1375–1393.
7 Y. Ma, S. Adjemian, S. R. Mattarollo, T. Yamazaki, L. Aymeric, H. Yang, J. P. Portela Catani, D. Hannani, H. Duret, K. Steegh, I. Martins, F. Schlemmer, M. Michaud, O. Kepp, A. Q. Sukkurwala, L. Menger, E. Vacchelli, N. Droin, L. Galluzzi, R. Krzysiek, S. Gordon, P. R. Taylor, P. Van Endert, E. Solary, M. J. Smyth, L. Zitvogel and G. Kroemer, *Immunity*, 2013, **38**, 729–741.
8 M. Obeid, A. Tesniere, F. Ghiringhelli, G. M. Fimia, L. Apetoh, J. L. Perfettini, M. Castedo, G. Mignot, T. Panaretakis, N. Casares, D. Metivier, N. Larochette, P. van Endert, F. Ciccosanti, M. Piacentini, L. Zitvogel and G. Kroemer, *Nat. Med.*, 2007, **13**, 54–61.
9 S. Spranger, H. K. Koblish, B. Horton, P. A. Scherle, R. Newton and T. F. Gajewski, *J. Immunother. Cancer*, 2014, **2**, 3–16.
10 M. A. Curran, W. Montalvo, H. Yagita and J. P. Allison, *Proc. Natl. Acad. Sci. U. S. A.*, 2010, **107**, 4275–4280.
11 M. Mandai, J. Hamanishi, K. Abiko, N. Matsumura, T. Baba and I. Konishi, *Clin. Cancer Res.*, 2016, **22**, 2329–2334.
12 A. J. Muller, J. B. DuHadaway, P. S. Donover, E. Sutanto-Ward and G. C. Prendergast, *Nat. Med.*, 2005, **11**, 312–319.
13 X. Liu, N. Shin, H. K. Koblish, G. Yang, Q. Wang, K. Wang, L. Leffet, M. J. Hansbury, B. Thomas, M. Rupar, P. Waeltz, K. J. Bowman, P. Polam, R. B. Sparks, E. W. Yue, Y. Li, R. Wynn, J. S. Fridman, T. C. Burn, A. P. Combs, R. C. Newton and P. A. Scherle, *Blood*, 2010, **115**, 3520–3530.
14 S. Spranger, R. M. Spaapen, Y. Zha, J. Williams, Y. Meng, T. T. Ha and T. F. Gajewski, *Sci. Transl. Med.*, 2013, **5**, 200ra116.
15 C. Uyttenhove, L. Pilotte, I. Theate, V. Stroobant, D. Colau, N. Parmentier, T. Boon and B. J. Van den Eynde, *Nat. Med.*, 2003, **9**, 1269–1274.
16 C. A. Opitz, U. M. Litzenburger, F. Sahm, M. Ott, I. Tritschler, S. Trump, T. Schumacher, L. Jestaedt, D. Schrenk, M. Weller, M. Jugold, G. J. Guillemin, C. L. Miller, C. Lutz, B. Radlwimmer, I. Lehmann, A. von Deimling, W. Wick and M. Platten, *Nature*, 2011, **478**, 197–203.
17 D. H. Munn and A. L. Mellor, *Trends Immunol.*, 2013, **34**, 137–143.
18 M. B. Fuertes, S. R. Woo, B. Burnett, Y. X. Fu and T. F. Gajewski, *Trends Immunol.*, 2013, **34**, 67–73.
19 Y. Chen, R. Xia, Y. Huang, W. Zhao, J. Li, X. Zhang, P. Wang, R. Venkataramanan, J. Fan, W. Xie, X. Ma, B. Lu and S. Li, *Nat. Commun.*, 2016, **7**, 13443–13454.
20 M. D. Sharma, R. Shinde, T. L. McGaha, L. Huang, R. B. Holmgaard, J. D. Wolchok, M. R. Mautino, E. Celis, A. H. Sharpe, L. M. Francisco, J. D. Powell, H. Yagita, A. L. Mellor, B. R. Blazar and D. H. Munn, *Sci. Adv.*, 2015, **1**, e1500845.
21 B. Ravishankar, H. Liu, R. Shinde, P. Chandler, B. Baban, M. Tanaka, D. H. Munn, A. L. Mellor, M. C. Karlsson and T. L. McGaha, *Proc. Natl. Acad. Sci. U. S. A.*, 2012, **109**, 3909–3914.
22 T. S. Johnson, T. McGaha and D. H. Munn, *Adv. Exp. Med. Biol.*, 2017, **1036**, 91–104.
23 D. H. Munn, M. D. Sharma and T. S. Johnson, *Cancer Res.*, 2018, **78**, 5191–5199.
24 V. P. Balachandran, M. J. Cavnar, S. Zeng, Z. M. Bamboat, L. M. Ocuin, H. Obaid, E. C. Sorenson, R. Popow, C. Ariyan, F. Rossi, P. Besmer, T. Guo, C. R. Antonescu, T. Taguchi, J. Yuan, J. D. Wolchok, J. P. Allison and R. P. DeMatteo, *Nat. Med.*, 2011, **17**, 1094–1100.

25 B. Feng, F. Zhou, B. Hou, D. Wang, T. Wang, Y. Fu, Y. Ma, H. Yu and Y. Li, *Adv. Mater.*, 2018, **30**, 1803001–1803010.
26 C. M. Hartshorn, M. S. Bradbury, G. M. Lanza, A. E. Nel, J. Rao, A. Z. Wang, U. B. Wiesner, L. Yang and P. Grodzinski, *ACS Nano*, 2018, **12**, 24–43.
27 T. Wang, D. Wang, H. Yu, B. Feng, F. Zhou, H. Zhang, L. Zhou, S. Jiao and Y. Li, *Nat. Commun.*, 2018, **9**, 1532–1543.
28 F. Zhou, B. Feng, H. Yu, D. Wang, T. Wang, Y. Ma, S. Wang and Y. Li, *Adv. Mater.*, 2019, **31**, 1805888–1805898.
29 D. Wang, T. Wang, J. Liu, H. Yu, S. Jiao, B. Feng, F. Zhou, Y. Fu, Q. Yin, P. Zhang, Z. Zhang, Z. Zhou and Y. Li, *Nano Lett.*, 2016, **16**, 5503–5513.
30 J. Lu, X. Liu, Y. P. Liao, F. Salazar, B. Sun, W. Jiang, C. H. Chang, J. Jiang, X. Wang, A. M. Wu, H. Meng and A. E. Nel, *Nat. Commun.*, 2017, **8**, 1811–1824.
31 J. Lu, X. Liu, Y. P. Liao, X. Wang, A. Ahmed, W. Jiang, Y. Ji, H. Meng and A. E. Nel, *ACS Nano*, 2018, **12**, 11041–11061.
32 D. Huang, H. Qian, H. Qiao, W. Chen, J. Feijen and Z. Zhong, *Expert Opin. Drug Delivery*, 2018, **15**, 703–716.
33 Q. Song, Y. Yin, L. Shang, T. Wu, D. Zhang, M. Kong, Y. Zhao, Y. He, S. Tan, Y. Guo and Z. Zhang, *Nano Lett.*, 2017, **17**, 6366–6375.
34 A. Jhaveri, P. Deshpande and V. Torchilin, *J. Controlled Release*, 2014, **190**, 352–370.
35 Y. Li, D. Maciel, J. Rodrigues, X. Shi and H. Tomas, *Chem. Rev.*, 2015, **115**, 8564–8608.
36 W. Chen, Y. Hou, Z. Tu, L. Gao and R. Haag, *J. Controlled Release*, 2017, **259**, 160–167.
37 M. Platten, W. Wick and B. J. Van den Eynde, *Cancer Res.*, 2012, **72**, 5435–5440.
38 Y. H. Peng, S. H. Ueng, C. T. Tseng, M. S. Hung, J. S. Song, J. S. Wu, F. Y. Liao, Y. S. Fan, M. H. Wu, W. C. Hsiao, C. C. Hsueh, S. Y. Lin, C. Y. Cheng, C. H. Tu, L. C. Lee, M. F. Cheng, K. S. Shia, C. Shih and S. Y. Wu, *J. Med. Chem.*, 2016, **59**, 282–293.
39 E. Vacchelli, F. Aranda, A. Eggermont, C. Sautes-Fridman, E. Tartour, E. P. Kennedy, M. Platten, L. Zitvogel, G. Kroemer and L. Galluzzi, *OncoImmunology*, 2014, **3**, e957994.
40 U. F. Rohrig, S. R. Majjigapu, P. Vogel, V. Zoete and O. Michielin, *J. Med. Chem.*, 2015, **58**, 9421–9437.
41 L. Galluzzi, A. Buque, O. Kepp, L. Zitvogel and G. Kroemer, *Nat. Rev. Immunol.*, 2017, **17**, 97–111.
42 I. Martins, Y. Wang, M. Michaud, Y. Ma, A. Q. Sukkurwala, S. Shen, O. Kepp, D. Metivier, L. Galluzzi, J. L. Perfettini, L. Zitvogel and G. Kroemer, *Cell Death Differ.*, 2014, **21**, 79–91.
43 W. Wang, S. Qin and L. Zhao, *Biomed. Pharmacother.*, 2015, **69**, 18–23.
44 J. W. Hodge, C. T. Garnett, B. Farsaci, C. Palena, K. Y. Tsang, S. Ferrone and S. R. Gameiro, *Int. J. Cancer*, 2013, **133**, 624–636.
45 Y. Chu, L. X. Wang, G. Yang, H. J. Ross, W. J. Urba, R. Prell, K. Jooss, S. Xiong and H. M. Hu, *J. Immunother.*, 2006, **29**, 367–380.
46 P. M. Arlen, J. L. Gulley, C. Parker, L. Skarupa, M. Pazdur, D. Panicali, P. Beetham, K. Y. Tsang, D. W. Grosenbach, J. Feldman, S. M. Steinberg, E. Jones, C. Chen, J. Marte, J. Schlom and W. Dahut, *Clin. Cancer Res.*, 2006, **12**, 1260–1269.
47 C. T. Garnett, J. Schlom and J. W. Hodge, *Clin. Cancer Res.*, 2008, **14**, 3536–3544.
48 J. Lu, X. Liu, Y. P. Liao, X. Wang, A. Ahmed, W. Jiang, Y. Ji, H. Meng and A. E. Nel, *ACS Nano*, 2018, **12**, 11041–11061.
49 M. Della Chiesa, S. Carlomagno, G. Frumento, M. Balsamo, C. Cantoni, R. Conte, L. Moretta, A. Moretta and M. Vitale, *Blood*, 2006, **108**, 4118–4125.
50 K. Cheng, Y. Ding, Y. Zhao, S. F. Ye, X. Zhao, Y. L. Zhang, T. J. Ji, H. H. Wu, B. Wang, G. J. Anderson, L. Ren and G. J. Nie, *Nano Lett.*, 2018, **18**, 3250–3258.
51 D. Marvel and D. I. Gabrilovich, *J. Clin. Invest.*, 2015, **125**, 3356–3364.

